JOURNAL OF Materials CHEMISTRY

High-temperature electrical transport in $La_{0.3}Sr_{0.7}Fe_{1-x}Ga_xO_{3-\delta}$ ($x = 0$–0.5)†

Ilia A. Leonidov,[a] Victor L. Kozhevnikov,[a] Edward B. Mitberg,[a] Mikhail V. Patrakeev,[b] Vladislav V. Kharton*[b] and Fernando M. B. Marques[b]

[a]*Institute of Solid State Chemistry, Ural Division of RAS, 91 Pervomaiskaia, Ekaterinburg 620219, Russia*
[b]*Department of Ceramics and Glass Engineering, UIMC, University of Aveiro, Aveiro 3810-193, Portugal. E-mail: kharton@cv.ua.pt*

Received 14th December 2000, Accepted 2nd February 2001
First published as an Advance Article on the web 2nd March 2001

The electrical properties of perovskite-related oxide $La_{0.3}Sr_{0.7}Fe_{1-x}Ga_xO_{3-\delta}$ ($x = 0$–0.5) are reported within the temperature range 750 to 950 °C and the oxygen partial pressure range between 10^{-19} and 0.5 atm. The maximum solid solubility of gallium in the iron sublattice of $La_{0.3}Sr_{0.7}FeO_{3-\delta}$ is close to 30%. At oxygen pressures about 10^{-4} atm, the materials undergo a transition from perovskite to oxygen vacancy ordered structures. The type of vacancy ordering depends on gallium content. Both p- and n-type electronic conductivities decrease when insulating gallium cations having stable oxidation state are incorporated into the iron sublattice of the ferrite. The observed temperature and oxygen pressure dependencies of the p-type electronic conductivity in the ordered phases suggest a transition from the intrinsic regime, when the electron–hole conduction is governed by the band gap, to the extrinsic regime, controlled by the amount of the oxygen excess in the vacancy ordered structure. The ordered strontium–lanthanum ferrite was shown to be a mixed conductor with oxygen ionic conductivity of about 0.1 S cm^{-1} at 900 °C. Ionic conduction in the vacancy ordered phases decreases with increasing gallium concentration.

1 Introduction

Mixed oxygen ionic–electronic conductors are of considerable interest as materials of ceramic membranes for the partial oxidation of methane to synthesis gas (syngas), a mixture of carbon monoxide and hydrogen.[1–4] Whilst the most significant cost associated with the conventional technologies of the partial oxidation of methane is that of an oxygen plant, using mixed-conductive membranes integrates oxygen separation, steam reforming and partial oxidation into a single step for natural gas conversion. The prospective membrane materials should satisfy numerous requirements, including structural and chemical stability in both oxidising and severe reducing conditions, a high oxygen semi-permeability and favourable thermomechanical properties. The highest oxygen permeability level is characteristic for perovskite-like oxides in the systems La–A–Co–O and La–A–Fe–O, where A is an alkaline earth element.[5–8] These phases are, however, thermodynamically and/or dimensionally unstable under large oxygen chemical potential gradients.[9–14] In case of cobaltites, $(La,Sr)CoO_{3-\delta}$, the accumulation of oxygen vacancies leads initially to the development of local defect clusters, then to structural reconstruction of the perovskite lattice,[9] and finally to reduction and destruction of the material at moderately low oxygen pressures.[10] Although Fe-containing phases are generally more robust than cobaltites, oxygen losses in reducing environments and concomitant changes in the oxidation state of iron cations result in very unfavourable lattice expansion, leading to ceramic membrane failures.[11–14]

The lattice instability of ferrites under large oxygen chemical potential gradients may be partially suppressed by substitution of iron with higher valence metal cations, such as Cr or Ti.[11,15] In particular, membranes of the doped derivative $La_{0.2}Sr_{0.8}Fe_{0.8}Cr_{0.2}O_{3-\delta}$ were successfully tested in syngas generation experiments for 500 h at 1100 °C.[11] However, doping with either chromium or titanium leads to a decrease of ionic conductivity and, hence, oxygen permeability of $SrFeO_{3-\delta}$-based materials.[16,17] In addition, segregation of secondary alkaline-earth chromite phases may occur in Cr-containing compositions, heavily doped in the A sublattice.[18–20] Another promising approach to improve stability of perovskite-related oxides under membrane operation conditions refers to isovalent doping with trivalent cations of stable oxidation state into the B sites.[12,14,21] For example, a significant oxygen permeability and sufficient stability were found for the compounds $Sr_{1-x}La_xFe_{1-y}Ga_yO_{3-\delta}$ ($x = 0.1$–0.4; $y = 0.2$–0.5), in which the crystal lattice was identified as brownmillerite-type.[12] Note, however, that charge compensation in the latter compounds requires a significantly larger oxygen content than that typical for brownmillerite, Ca_2AlFeO_5, especially in oxidising conditions when a considerable part of iron exists in tetravalent state.[22] The present work, continuing our research focused on transport properties of $SrFeO_{3-\delta}$-based materials,[17,22,23] is aimed at analysis of electronic and ionic conduction in the oxide compounds $La_{0.3}Sr_{0.7}Fe_{1-x}Ga_xO_{3-\delta}$ ($x = 0$–0.5).

2 Experimental

The powder specimens $La_{0.3}Sr_{0.7}Fe_{1-x}Ga_xO_{3-\delta}$, where $x = 0$, 0.1, 0.2, 0.3, 0.4 and 0.5, were prepared by a solid-state reaction method from appropriate amounts of high purity grade La_2O_3, Fe_2O_3, Ga_2O_3 and $SrCO_3$. The starting reagents were calcined for 10 h at 600 °C, weighed in a dry box, ball milled and fired at 900–1100 °C in air during 30 h with intermittent grindings.

†Electronic supplementary information (ESI) available: XRD patterns for $La_{0.3}Sr_{0.7}Fe_{1-x}Ga_xO_{3-\delta}$. See http://www.rsc.org/suppdata/jm/b0/b009979l/

Ceramic samples with densities of about 90% of the theoretical density were obtained by sintering at 1200 °C in air. Prior to X-ray diffraction (XRD) studies, the specimens were annealed in air at 1200 °C for 18 hours and then slowly cooled during approximately 20 h. Such a treatment was aimed to obtain oxygen contents as close as possible to the equilibrium values. The X-ray powder diffraction data were collected on a Rigaku Geigerflex diffractometer (CuK_α radiation) over the range $10^\circ \leqslant 2\theta \leqslant 110^\circ$ using a stepwidth of 0.02°; collection time for every sample was approximately 10 h. Crystal structures were refined by the Rietvield method using the program FULL-PROF.[24] Variations in the oxygen nonstoichiometry of the samples were studied using the coulometric titration technique; a detailed description of the equipment and experimental procedure of the coulometric titration has been published elsewhere.[25]

The total conductivity (σ) was measured using the four-probe DC technique, as described elsewhere.[26] The measurements were carried out in a device with the sample holder being placed into an yttria-stabilized zirconia (YSZ) cell comprising an electrochemical oxygen pump and a sensor.[26] At the start of the experiment, the cell was filled with a gas mixture containing 50% of O_2 and 50% of CO_2 and then sealed. The conductivity was measured using a voltmeter Solartron 7081 in the temperature range 750 to 950 °C at oxygen partial pressures from 10^{-19} to 0.5 atm. Precise variation or maintenance of the partial oxygen pressure in the chamber was provided by the operation of the oxygen pump and sensor, controlled by a computer using specially developed software. The measurements were carried out in the mode of decreasing oxygen partial pressure in isothermal runs. When maintaining a constant oxygen pressure in the well-known instability range,[27] corresponding to the electrochemical sensor e.m.f. from approximately 200 to 650–700 mV, the operation regime of the oxygen pump utilised provided the sensor e.m.f. constant with an accuracy of ± 2 mV. Experimental data points were collected upon achievement of equilibrium between the sample and ambient atmosphere; the criterion of the equilibrium achieved was a conductivity relaxation rate less than 0.1% per minute, under a fixed oxygen pressure inside the chamber. The conductivity relaxation time after a change in the oxygen pressure over a sample varied up to several dozen hours, depending on temperature, oxygen partial pressure and cation composition. As a rule, the conductivity relaxation time in the instability range was no less than 1 hour; the total time necessary for one isothermal measurement cycle was 20–70 hours. The above-described criteria are believed to ensure that the obtained conductivity data correspond to equilibrium oxygen content in the samples. Upon achievement of the desirable low oxygen-pressure limit, the measurements were halted and then the oxygen pressure was increased to the starting upper limit, where the measurements were repeated in order to confirm reversibility of the experiment; thereupon temperature was changed thus enabling next measuring cycle.

3 Results and discussion

3.1 Structure

The room temperature XRD spectra of $La_{0.3}Sr_{0.7}Fe_{1-x}Ga_xO_{3-\delta}$, equilibrated with atmospheric air, showed the formation of a single perovskite-like phase within the composition range $0 \leqslant x \leqslant 0.3$; the crystal structure was preliminarily identified as cubic. Increasing gallium concentration results in a segregation of the secondary phase $SrLaGa_3O_7$.[28] For the compositions with $x = 0.4$ and 0.5, the content of the strontium–lanthanum gallate impurity phase was estimated from the XRD data to be about 5 and 12%, respectively. The perovskite unit cell parameters increase with gallium addition (Table 1); this behaviour is similar to that of Fe-doped $La(Sr)Ga(Mg)O_{3-\delta}$ perovskite solid solutions[29] and $(Sr,La)(Fe,Ga)O_{3-\delta}$ phases claimed to be brownmillerites.[12] One should note that trivalent iron cations in perovskite-like ferrites were reported to exist in the high-spin state.[30,31] Ionic radii of high-spin 4- and 5-coordinated Fe^{3+} as well as the radius of octahedrally-coordinated Fe^{4+} are less that that of Ga^{3+} in the octahedral coordination, while the ionic radius of octahedrally-coordinated Fe^{3+} is larger than that of gallium.[32] Therefore, the enlargement of the unit cell volume with increasing gallium concentration in $La_{0.3}Sr_{0.7}Fe_{1-x}Ga_xO_{3-\delta}$ at $0 \leqslant x \leqslant 0.3$ may be related to replacement of 4- and 5-coordinated Fe^{3+} and octahedrally-coordinated Fe^{4+} with gallium cations. According to the results of coulometric titration, briefly discussed below, the fraction of tetravalent iron in the studied temperature range in air varies from 10 to approximately 40%. On the other hand, the existence of ordered brownmillerite-like microdomains with tetrahedral coordination of Fe^{3+} is characteristic of strontium ferrite, when the oxygen content $(3-\delta)$ is intermediate between values typical for perovskite and brownmillerite phases.[33] An additional factor, affecting the increase in lattice parameter with increasing x, refers to increasing coulombic repulsion of the cations with decreasing oxygen content in the lattice (for example, ref. 34). Finally, when the gallium concentration in $La_{0.3}Sr_{0.7}Fe_{1-x}Ga_xO_{3-\delta}$ exceeds the solid solution formation limit (*i.e.* $x > 0.3$), further increase of the perovskite lattice parameter with x is due to changing ratio La : Sr in the perovskite phase, resulting from the gallate $SrLaGa_3O_7$ formation.

It should also be mentioned that a slight broadening of peaks at high 2θ angles on the XRD patterns of the title materials equilibrated with atmospheric air may indicate a crystal symmetry lower than primitive cubic. For instance, the rhombohedrally-distorted perovskite structure is characteristic of the oxidized form of the $Sr_2LaFe_3O_{9-\delta}$ compound.[35] This fact and the complexity of the lattice changes at reduced oxygen pressures necessitate a more detailed structural investigation, which is now in progress. The conclusions on the structure of the title materials, made in the present paper, should therefore be considered only as preliminary. However, the discussed structural features, including the changes in the unit cell volume as a function of gallium content and the phase transitions, are believed to correctly reflect the behaviour of the ferrite–gallate phases.

The XRD pattern of $La_{0.3}Sr_{0.7}FeO_{3-\delta}$ quenched at $p(O_2) = 10^{-14}$ atm from 750 °C to room temperature shows an orthorhombic brownmillerite-like structure (S.G. *Pmma*); a similar spectrum was obtained for the material quenched at $p(O_2) = 10^{-8}$ atm. The unit cell parameters (Table 1), related to the perovskite parameter (a_p) as $a = \sqrt{2} \times a_p$, $b = 3 \times a_p$, $c = \sqrt{2} \times a_p$, are found to be comparable to those reported by Battle *et al.*[36] for the reduced form of the $Sr_2LaFe_3O_{9-\delta}$ compound. This lattice can be described as consisting of layers of iron–oxygen octahedra (O) and tetrahedra (T) ordered as …OOTOOT… along the *b*-axis of the unit cell. Note that the alteration of the layers in the structure of $La_{0.3}Sr_{0.7}FeO_{3-\delta}$, observed at low oxygen pressures, differs from the stacking sequence …OTOTO… particular to the brownmillerite structure. The Ga-containing phases quenched in the same conditions exhibit another structure, which may not be interpreted as brownmillerite-like. Examples are given in the Electronic Supplementary Information,† demonstrating considerable differences between the XRD patterns of the quenched $La_{0.3}Sr_{0.7}Fe_{0.9}Ga_{0.1}O_{3-\delta}$, quenched $La_{0.3}Sr_{0.7}FeO_{3-\delta}$ and brownmillerite $SrFeO_{2.5}$. The lattice of quenched samples $La_{0.3}Sr_{0.7}Fe_{1-x}Ga_xO_{3-\delta}$ ($x = 0.1$–0.3) was identified as orthorhombic (S.G. *Pmmm*, $a = 2\sqrt{2} \times a_p$, $b = 2a_p$, $c = \sqrt{2} \times a_p$), close to the low temperature modification of the ferrite $SrFeO_{2.75}$ recently described in space group *Pmma*.[37] The crystal structure of the reduced phases $La_{0.3}Sr_{0.7}(Fe,Ga)O_{3-\delta}$

Table 1 Unit cell parameters of $La_{0.3}Sr_{0.7}Fe_{1-x}Ga_xO_{3-\delta}$, as-prepared and quenched at $pO_2 = 10^{-14}$ atm from 750 °C to room temperature

Parameter/ Å	x in $La_{0.3}Sr_{0.7}Fe_{1-x}Ga_xO_{3-\delta}$					
	0	0.1	0.2	0.3	0.4	0.5
As-prepared						
a	3.873(1)	3.876(8)	3.882(8)	3.893(8)	3.902(0)	3.907(1)
Quenched						
a	5.498(7)	11.116(0)	11.168(0)			
b	11.867(9)	7.845(2)	7.847(2)			
c	5.576(6)	5.548(7)	5.551(1)			

can be viewed as consisting from the layers where metal–oxygen octahedra are linked *via* corners with square metal–oxygen pyramids; the layers alternate along the *b*-axis so that the pyramids in the neighbouring layers share apex oxygen ions. The oxygen content in the samples with $x = 0.1$, 0.2 and 0.3 in the above-mentioned conditions of quenching was determined close to about 2.65, nearly independent also of the level of gallium doping. The oxygen stoichiometry is smaller than the value 2.75 expected from the structural consideration, which may be interpreted as evidence for the formation of random oxygen vacancies located most probably in the FeO_x polyhedra. Such an assumption is supported by the increase in the unit cell parameters with increasing gallium concentration (Table 1), since ionic radii of 5- and 6-coordinated Ga^{3+} are smaller than that of high-spin Fe^{3+} in the same coordination, but larger when the coordination number of gallium exceeds the coordination number of iron.[32]

3.2 Total electrical conductivity

Fig. 1 presents an example of typical data on the total electrical conductivity as a function of oxygen partial pressure at different temperatures, measured for the material with $x = 0.2$. The influence of the gallium doping on the conductivity at 800 and 950 °C is illustrated by Fig. 2. One can see that a smooth dependence of the total conductivity on oxygen pressure, characteristic of many oxide mixed conductors exhibiting both p- and n-type electronic conduction, is observed in the case of $La_{0.3}Sr_{0.7}Fe_{1-x}Ga_xO_{3-\delta}$ only at higher temperatures. The data obtained in the temperature range below 900 °C reveal peculiar changes in the conductivity in the oxygen pressure interval $10^{-10} < p(O_2) < 10^{-4}$ atm, discussed below. Fig. 3 shows the interrelation between the variation of oxygen content ($\Delta\delta$), related to that in atmospheric air, and the total conductivity of

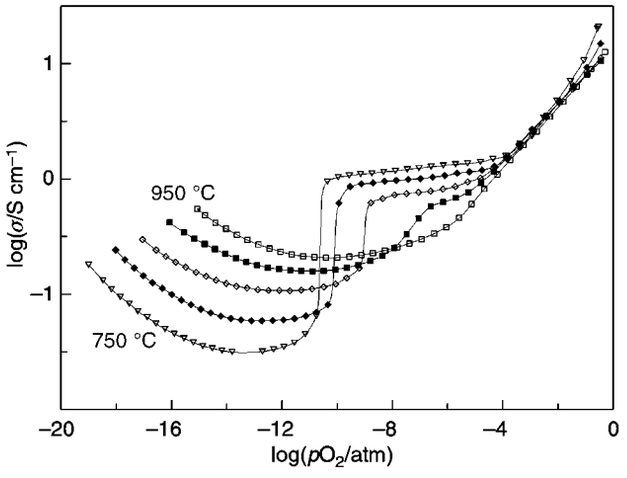

Fig. 1 The variations of the total conductivity of $La_{0.3}Sr_{0.7}Fe_{0.8}Ga_{0.2}O_{3-\delta}$ with temperature and oxygen partial pressure. The step between the conductivity isotherms is 50 °C. Solid lines are for visual guidance only.

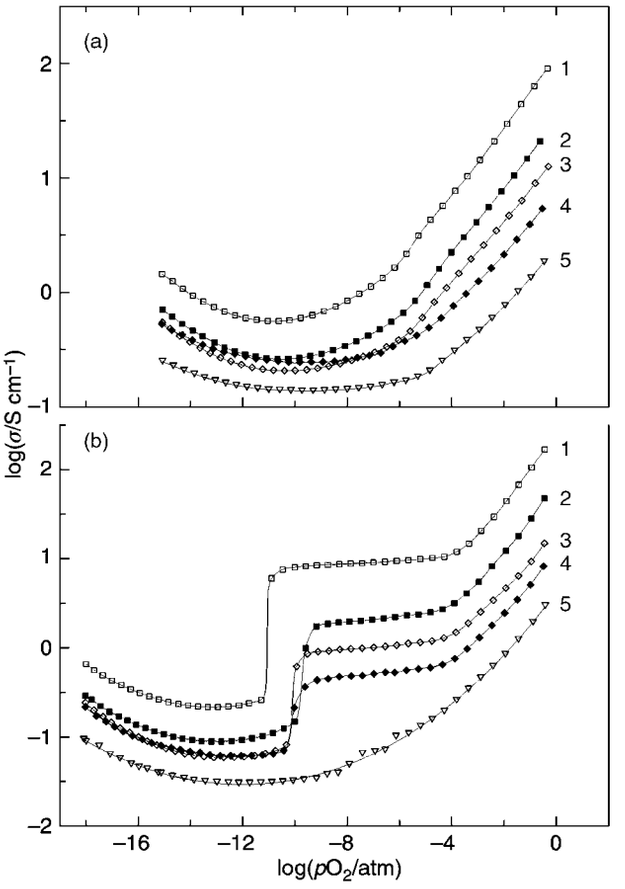

Fig. 2 Oxygen partial pressure dependences of the total conductivity of $La_{0.3}Sr_{0.7}Fe_{1-x}Ga_xO_{3-\delta}$ at 950 °C (a) and 800 °C (b). Numbers 1, 2, 3, 4 and 5 correspond to the x values equal to 0, 0.1, 0.2, 0.4 and 0.5, respectively. Solid lines are for visual guidance only.

$La_{0.3}Sr_{0.7}Fe_{1-x}Ga_xO_{3-\delta}$ ($x = 0$, 0.2 and 0.4) at 800 °C. Increasing oxygen partial pressure at $p(O_2) > 10^{-4}$ atm, when the title materials possess the perovskite-type structure, results in increasing conductivity nearly proportional to $p(O_2)^{+1/4}$, indicating a dominance of p-type electronic charge carriers. These changes in the total conductivity follow the increase in the oxygen content at $p(O_2) > 10^{-4}$ atm (Fig. 3).

At lower oxygen pressures where the structures with ordered oxygen vacancies become more stable, only a slight variation in the total conductivity of $La_{0.3}Sr_{0.7}Fe_{1-x}Ga_xO_{3-\delta}$ is observed on decreasing the oxygen partial pressure to about 10^{-10} atm

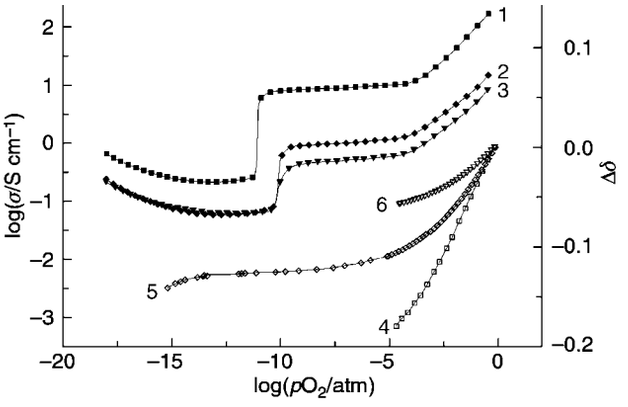

Fig. 3 Oxygen partial pressure dependences of the total conductivity (closed symbols) and the relative change in the oxygen content with respect to atmospheric air (open symbols) in $La_{0.3}Sr_{0.7}Fe_{1-x}Ga_xO_{3-\delta}$ at 800 °C: 1 and 4, $x = 0$; 2 and 5, $x = 0.2$; 3 and 6, $x = 0.4$.

(Figs. 1–3). Notice that in nonstoichiometric $SrFeO_{3-\delta}$ the transition from the perovskite to ordered phases occurs at $p(O_2) < (10^{-3.5}–10^{-4})$ atm and temperatures below 850 °C.[38,39] These conditions are quite close to those where the flat behaviour on the conductivity curves of $La_{0.3}Sr_{0.7}(Fe,Ga)O_{3-\delta}$ is observed to initiate. Hence, the appearance of the flat behaviour on reduction of the title materials is probably associated with the phase transitions. Further reduction of oxygen chemical potential ($p(O_2) \leqslant 10^{-10}$ atm) leads to a sharp, step-like decrease in the conductivity with the magnitude depending mainly on temperature and gallium concentration. As for the conductivity values, the jump magnitude decreases with gallium content; the nature of such behaviour is analysed below. It should be mentioned that the oxygen content in the samples remains practically invariable, *i.e.* $\Delta\delta << 3$, in the fairly wide range of $p(O_2)$ comprising the pressure of the conductivity jump. Only at oxygen pressures as low as 10^{-14}–10^{-15} atm does the oxygen content begin to decrease again while the conductivity begins to simultaneously increase with decreasing oxygen pressure, approaching asymptotically the $p(O_2)^{-1/4}$ proportionality law. Such an increase in the conductivity is indicative of n-type electron carriers prevailing in the low oxygen pressure limit.

The analysis of the oxygen partial pressure dependences of the conductivity isotherms in the vicinity of the low oxygen-pressure minima leads to a classical expression for a mixed oxygen ionic–electronic conductor

$$\sigma(T,pO_2) = \sigma_i^o(T) + \sigma_n^o(T)pO_2^{-1/4} + \sigma_p^o(T)pO_2^{+1/4} \qquad (1)$$

where the indexes i, n and p are related to the ion, electron and electron–hole components of the total conductivity, respectively, and σ_j^o (j = n, p, i) corresponds to the values of partial conductivities extrapolated to unit oxygen pressure. Table 2 lists the values of these parameters at different temperatures, obtained by fitting eqn. (1) to the experimental conductivity isotherms in the oxygen pressure range below the conductivity jumps. A comparison of the experimental data points with the calculated total conductivity is shown for the sample $x = 0.1$ as an example in Fig. 4. Fig. 5 presents the Arrhenius dependences of several transport parameters obtained from the fitting results, including the oxygen ionic conductivity (σ_i), the n-type electronic conductivity at $p(O_2) = 10^{-16}$ atm, and the minimum electron conductivity ($\sigma_{np\ min}$). For a given temperature, the latter quantity represents the minimum value of the sum of n- and p-type conductivities (σ_n and σ_p) at the oxygen partial pressure when $\sigma_n = \sigma_p$. The physical meaning of the minimum electron conductivity is discussed below.

3.3 n- and p-type electronic conduction

The isothermal plots of the sum of partial p- and n-type electronic conductivities ($\sigma_{np} = \sigma_n + \sigma_p$), obtained by subtraction of the ionic conductivity from the total conductivity values, are shown in Fig. 6. The slope of the electronic conductivity isotherms approaches −1/4 and +1/4 at $p(O_2)$ values to the left and right of the minima, respectively. This behaviour is characteristic of a nonstoichiometric semiconductor. Generation of the conducting electrons in the oxides may be explained by the loss of the lattice oxygen in the low oxygen pressure limit $O^{2-} \rightleftharpoons \frac{1}{2}O_2 + 2e^-$

$$K_n = \frac{[e^-]^2 pO_2^{1/2}}{[O^{2-}]} = K_n^o \exp\left[-\frac{\Delta H_n}{kT}\right] \qquad (2)$$

Here, K_n^o is constant and ΔH_n is the reaction enthalpy. Experimentally observed changes in the occupation of the oxygen sublattice in the vicinity of the conductivity minima are much smaller in comparison with the total concentrations of oxygen ions and vacancies (Fig. 3). Hence, neglecting the mobility activation energy for electrons, the classical power dependence $\sigma_n \sim [e^-] \sim p(O_2)^{-1/4}$, consistent with the experimental results, follows from the equilibrium constant. Also, the activation energy for the n-type electronic conductivity, E_n, should be about $\Delta H_n/2$. The values of E_n and ΔH_n, calculated from the Arrhenius plots of the electronic conductivity at $p(O_2) = 10^{-16}$ atm (Fig. 5b), are given in Table 3.

Within the limits of experimental error, the values of the activation energy for the n-type conduction in $La_{0.3}Sr_{0.7}Fe_{1-x}Ga_xO_{3-\delta}$ are approximately equal, varying in the narrow range from 1.8 to 1.9 eV. At the same time, the electronic conductivity of the undoped brownmillerite-like ferrite $La_{0.3}Sr_{0.7}FeO_{3-\delta}$ is about two times larger than that in the gallium-doped derivatives

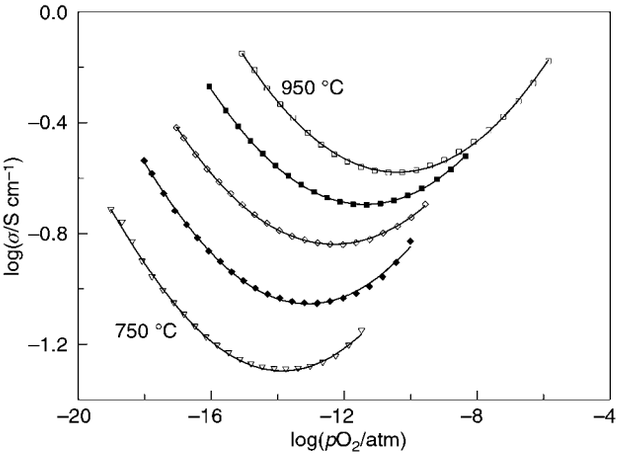

Fig. 4 Comparison of the experimental values of the total conductivity and fitting results (solid lines) for $La_{0.3}Sr_{0.7}Fe_{0.9}Ga_{0.1}O_{3-\delta}$. The step between the conductivity isotherms is 50 °C.

Table 2 Parameters of the regression model eqn. (1) for the total electrical conductivity in $La_{0.3}Sr_{0.7}Fe_{1-x}Ga_xO_{3-\delta}$

Gallium content, x	Conductivity parameter	Temperature/°C				
		950	900	850	800	750
0	σ_i^o	0.386	0.283	0.221	0.155	0.100
	σ_n^o	$1.8\cdot10^{-4}$	$8.2\cdot10^{-5}$	$3.4\cdot10^{-5}$	$1.5\cdot10^{-5}$	$5.9\cdot10^{-6}$
	σ_p^o	43.7	60.8	64.0	62.0	60.9
0.1	σ_i^o	0.195	0.150	0.109	0.062	0.034
	σ_n^o	$8.7\cdot10^{-5}$	$3.7\cdot10^{-5}$	$1.5\cdot10^{-5}$	$7.0\cdot10^{-6}$	$2.8\cdot10^{-6}$
	σ_p^o	13.7	18.1	21.3	24.5	23.9
0.2	σ_i^o	0.165	0.124	0.0829	0.0394	0.0187
	σ_n^o	$6.3\cdot10^{-5}$	$2.9\cdot10^{-5}$	$1.2\cdot10^{-5}$	$5.9\cdot10^{-6}$	$2.7\cdot10^{-6}$
	σ_p^o	7.24	10.3	12.5	14.2	14.1
0.4	σ_i^o	0.220	0.152	0.095	0.050	0.026
	σ_n^o	$5.3\cdot10^{-5}$	$2.3\cdot10^{-5}$	$9.7\cdot10^{-6}$	$4.9\cdot10^{-6}$	$2.1\cdot10^{-6}$
	σ_p^o	3.47	5.78	6.64	6.84	6.78

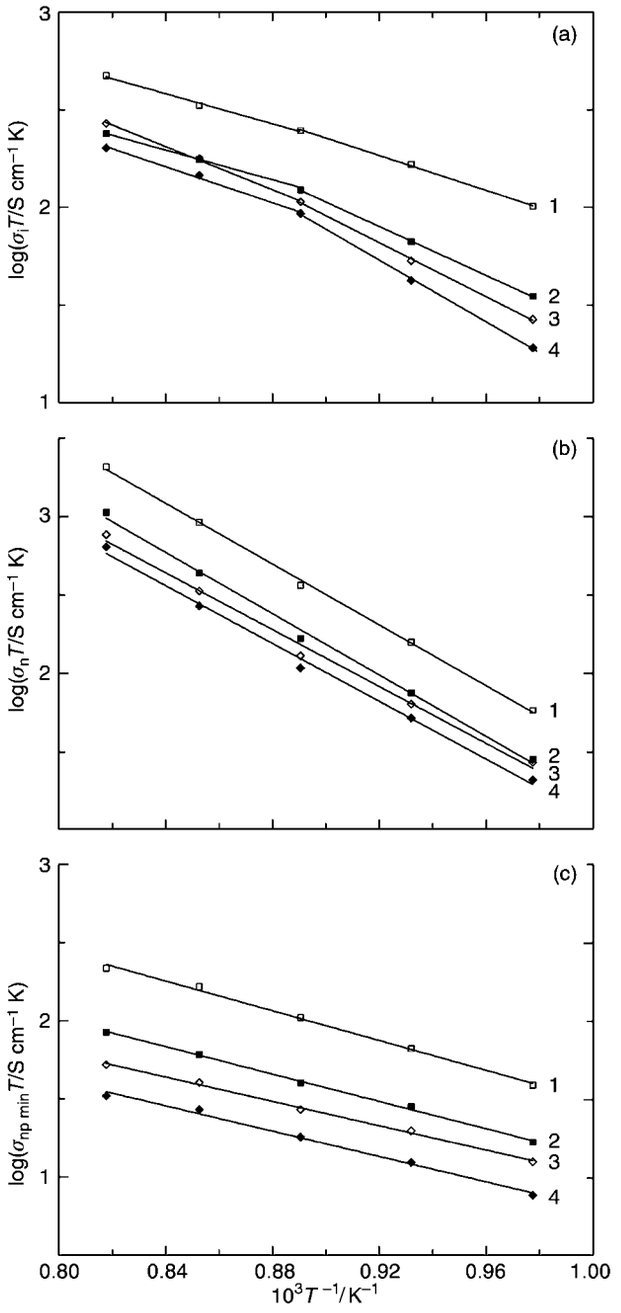

Fig. 5 Arrhenius plots for the oxygen ionic conductivity of $La_{0.3}Sr_{0.7}Fe_{1-x}Ga_xO_{3-\delta}$ at oxygen pressures below 10^{-10} atm (a), and n-type electronic conductivity at $p(O_2)=10^{-16}$ atm (b), and the minimum electronic conductivity (c). Numbers 1, 2, 3 and 4 correspond to the x values equal to 0, 0.1, 0.2 and 0.4, respectively.

(Fig. 5b). The decrease in the n-type conductivity with increasing gallium content results from a decrease in the electron mobility when iron structural sites, over which the electron transfer takes place, are occupied with insulating Ga cations having stable oxidation states. Similar behaviour was observed for the p-type electronic transport in $La(Co,Ga)O_{3-\delta}$ solid solutions.[40]

The hole conductivity increasing with the oxygen pressure after the minima in Fig. 7 is a result of the oxygen incorporation reaction $\frac{1}{2}O_2 \rightleftharpoons O^{2-} + 2h^+$

$$K_p = \frac{[h^+]^2[O^{2-}]}{pO_2^{1/2}} = K_p^o \exp\left[-\frac{\Delta H_p}{kT}\right] \quad (3)$$

where ΔH_p is the reaction enthalpy. Again, in the conditions of a small variation of the total oxygen content, electron–hole conductivity should increase with the oxygen pressure as $\sigma_p \sim [h^+] \sim p(O_2)^{1/4}$. This model is in agreement with the obtained results, as shown in Figs. 3 and 6. The p-type conductivity at $p(O_2)=1$ atm (σ_p^o), obtained by fitting using eqn. (1), exhibit a very weak dependence on temperature (Table 2); such behaviour suggests the values of the enthalpy ΔH_p to be fairly small. If neglecting the mobility activation for the electron holes, the weak increase in σ_p^o with decreasing temperature may indicate that the oxidation reaction (3) is slightly exothermic, *i.e.* $\Delta H_p < 0$. As for the n-type conductivity, the electron–hole conductivity in $La_{0.3}Sr_{0.7}Fe_{1-x}Ga_xO_{3-\delta}$ decreases with gallium additions due to blocking electron transfer by the stable Ga^{3+} cations.

The high-temperature equilibrium of electrons and holes near the conductivity minimum (Fig. 6) may be expressed as $0 \rightleftharpoons e^- + h^+$

$$K_i = [h^+][e^-] = K_i^o \exp\left[-\frac{E_g}{kT}\right] \quad (4)$$

where E_g is the band gap, and K_i^o is constant. The band gap may be estimated from the temperature dependence of the minimum electron conductivity ($\sigma_{np\ min}$). Expressing concentrations of electrons and holes *via* the partial conductivities and respective mobilities, μ_n and μ_p, one can rearrange eqn. (4) into the form

$$K_i = K_i^o \exp\left[-\frac{E_g}{kT}\right] = \left(\frac{\sigma_{np\ min}}{2e(\mu_n\mu_p)^{1/2}}\right)^2 \quad (5)$$

Presuming temperature-activated mobility for both electrons and electron holes

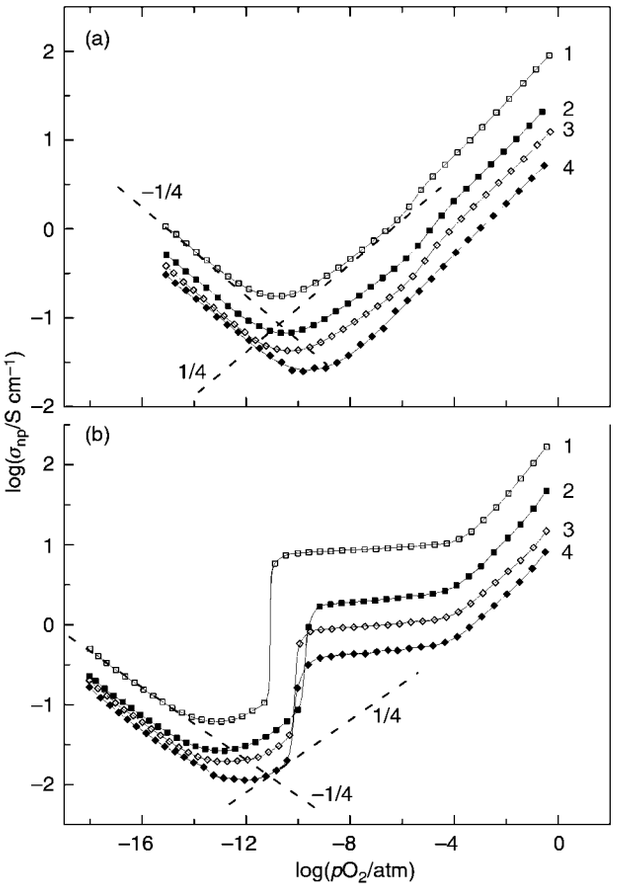

Fig. 6 Oxygen partial pressure dependences of the electron conductivity ($\sigma_{np}=\sigma_n+\sigma_p$) in $La_{0.3}Sr_{0.7}Fe_{1-x}Ga_xO_{3-\delta}$ at 950 °C (a) and 800 °C (b). Numbers 1, 2, 3 and 4 correspond to the x values equal to 0, 0.1, 0.2 and 0.4, respectively.

Table 3 The activation energies for the minimum electronic conductivity, partial n-type conductivity, the estimated band gap and enthalpy of the oxygen depletion reaction (2) in $La_{0.3}Sr_{0.7}Fe_{1-x}Ga_xO_{3-\delta}$

x	E_{np}/eV	E_g/eV	E_n/eV	ΔH_n/eV
0.0	0.94±0.03	1.88±0.06	1.92±0.04	3.84±0.08
0.1	0.87±0.02	1.74±0.04	1.93±0.06	3.9±0.1
0.2	0.77±0.02	1.54±0.04	1.79±0.08	3.6±0.2
0.4	0.80±0.04	1.60±0.08	1.82±0.07	3.6±0.1

$$\mu_{n,p} = \frac{\mu^{o}_{n,p}}{T}\exp\left[-\frac{\varepsilon_{n,p}}{kT}\right] \quad (6)$$

where ε_n and ε_p are the mobility activation energies for electrons and holes, respectively, the value of $(E_g+\varepsilon_n+\varepsilon_p)\equiv E_{np}$ can be found from the plots of $\log(\sigma_{np\ min}\times T)$ *versus* reciprocal temperature (Fig. 5c). For the title materials, the parameter E_{np} decreases with increasing gallium content (Table 3). Note that the activation energy for migration of both electrons and holes in lanthanum-rich $Sr_{1-x}La_xFeO_{3-\delta}$ ($x=0.75$–1.0) was reported to be nearly zero.[41,42] If one assumes the activation energies for the electronic charge carrier mobility in the Sr-rich compounds $La_{0.3}Sr_{0.7}Fe_{1-x}Ga_xO_{3-\delta}$ to be also negligibly small, one can obtain $E_g \approx 2E_{np}$. The estimated values of the band gap, E_g, are listed in Table 3. As for the enthalpy ΔH_n, the values of E_g decrease from 1.88 to 1.60 eV when the gallium concentration increases. This correlation seems quite reasonable as both reactions (2) and (3) result in a transition of bound electron to a mobile state.

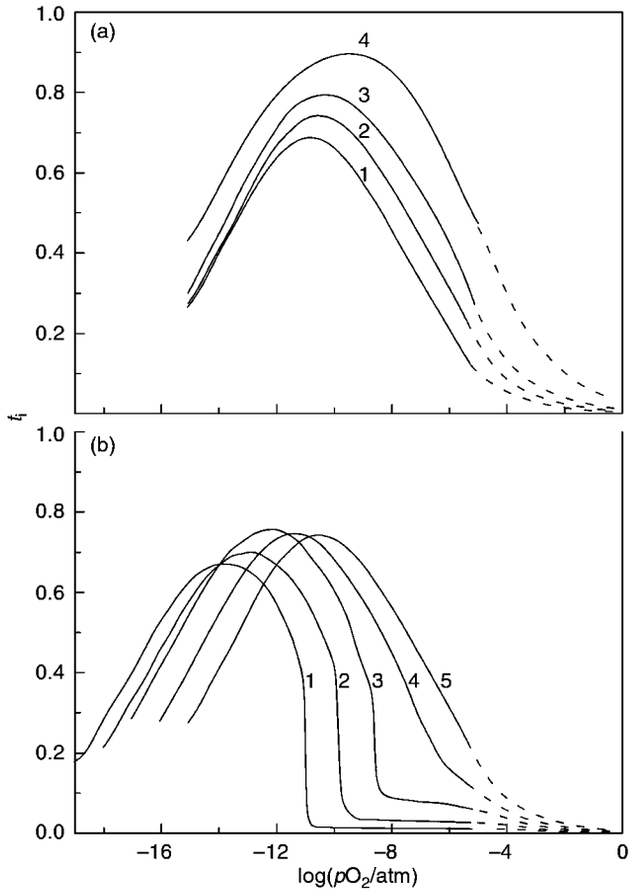

Fig. 7 Oxygen partial pressure dependences of the ion transference numbers: (a) $La_{0.3}Sr_{0.7}Fe_{1-x}Ga_xO_{3-\delta}$ at 950 °C: (1) $x=0$; (2) $x=0.1$; (3) $x=0.2$; (4) $x=0.5$. (b) $La_{0.3}Sr_{0.7}Fe_{0.9}Ga_{0.1}O_{3-\delta}$ at (1) 750 °C; (2) 800 °C; (3) 850 °C; (4) 900 °C; (5) 950 °C. The dashed lines were calculated under the assumption that the phase changes with increasing oxygen pressure have no effect on ionic conductivity.

Another interesting feature of the conductivity behaviour refers to the jump-like change in the hole contribution. This variation may be interpreted as evidence of a fast shift of the Fermi level from a near mid-gap position to the top of the valence band, resulting from an appearance of impurity-like acceptor states just above the top of the valence band, when the oxygen content increases. The amount of oxygen necessary to incite the impurity states is quite small. For instance, it can be estimated from Fig. 3 that the critical value of the oxygen excess $\Delta\delta$ with respect to the oxygen content, corresponding to the minimum of electronic conductivity in $La_{0.3}Sr_{0.7}Fe_{1-x}Ga_xO_{3-\delta}$, is about 0.01. A similar jump is observed in the brownmillerite $SrFeO_{2.5+\delta}$ where the oxygen excess $0.01<\delta<0.05$ leads to the transition of electron conductivity from the intrinsic to impurity controlled regime.[23] In the regime controlled by the impurity states, the conductivity level is governed mainly by the concentration of acceptor centres. Considering nearly flat portions of the isotherms in Fig. 1 corresponding to the impurity-controlled regime in $La_{0.3}Sr_{0.7}Fe_{1-x}Ga_xO_{3-\delta}$, one can conclude that increasing oxygen pressure up to about 10^{-4} atm results in only a minute increase in the concentration of acceptors. At the same time, the temperature decrease from 900 to 750 °C at $pO_2=10^{-6}$ atm increases the level of conductivity by about half an order of magnitude.

The influence of cation composition on the conductivity is distinctly seen in Fig. 6b. The increase of gallium content in $La_{0.3}Sr_{0.7}Fe_{1-x}Ga_xO_{3-\delta}$ from $x=0$ to $x=0.4$ results in the decrease of the impurity-controlled conductivity level by about one and a half orders of magnitude. Most probably, this decrease is a consequence of the respective decrease in the hole mobility because of the decrease in the amount of iron–oxygen structural polyhedra over which hole conduction takes place. The oxygen pressure increase above about 10^{-4} atm results in a smooth increase in the hole conductivity, related either to a change in the electronic band structure due to the phase transition to the perovskite structure or to a merge of the impurity states with the electronic states at the top of the valence band. The above consideration suggests relevance of the impurity levels and electron states of the oxygen incorporated in the structure and essential p-character of electron holes. Such a conclusion is corroborated by recent studies of electron energy loss spectra in the solid solutions $SrTi_{1-x}Fe_xO_{3-\delta}$[43] and Mössbauer measurements for oxygen vacancy ordered ferrites $Sr_nFe_nO_{3n-1}$.[37]

3.4 Oxygen ionic transport

Arrhenius plots for the oxygen ionic conductivity of $La_{0.3}Sr_{0.7}Fe_{1-x}Ga_xO_{3-\delta}$, calculated using eqn. (1) for oxygen pressures below 10^{-10} atm, are presented in Fig. 5a; Table 4 lists the values of the activation energy for ionic conductivity in different temperature ranges. Decreasing the temperature to about 850 °C results in a considerable increase in the activation energy, indicating probably a transition from partially disordered to oxygen-vacancy ordered structures. This behaviour is in excellent agreement with the data on phase changes in $La_{0.3}Sr_{0.7}(Fe,Ga)O_{3-\delta}$, discussed above. Doping with gallium leads to decreasing ionic conductivity of $La_{0.3}Sr_{0.7}Fe_{1-x}Ga_xO_{3-\delta}$ ($x=0$–0.2) in the low oxygen partial pressure range, in agreement with the literature;[12] the activation energy for oxygen ionic conduction increases with gallium additions. At larger x, the La : Sr cation concentration ratio in the solid solution decreases with increasing x due to the $SrLaGa_3O_7$ phase segregation. While the amount of segregated $SrLaGa_3O_7$ phase is moderate and has no significant effect on ionic transport, the decrease in La : Sr ratio leads to a slight increase in the ionic conductivity values (Fig. 6a).

The difference in the values of ionic conductivity and the activation energy, observed between undoped $La_{0.3}Sr_{0.7}FeO_{3-\delta}$

and Ga-containing materials, is quite large, especially at temperatures below 850 °C. One can therefore conclude that the brownmillerite-like structure acquired by the ferrite $La_{0.3}Sr_{0.7}FeO_{3-\delta}$ at low oxygen pressures, *i.e.* at large loss of lattice oxygen, is more favorable for the ion transfer than the oxygen-vacancy ordered structure formed in the case of doped $La_{0.3}Sr_{0.7}Fe_{1-x}Ga_xO_{3-\delta}$ ($x>0$). The conductivity variations with gallium content and changing crystal lattice may be explained as resulting from changes in the size of the bottleneck available for the jumping oxygen ion. In other words, every elementary jump of an oxygen ion to the nearby oxygen vacancy is through the space framed by two A-site cations (La/Sr) and one B-site cation (Fe/Ga), called a bottleneck. A draft assessment of the migration channel size can be deduced from the unit cell parameters (Table 1). In particular, if one considers the perovskite unit cell parameters (a_p) as a measure for the bottleneck size, the value $a_p=b/3$ equals about 3.95 Å in the brownmillerite-like structure of $La_{0.3}Sr_{0.7}FeO_{3-\delta}$, which is larger than $a_p=b/2\approx3.92$ Å in the vacancy-ordered structure of gallium-doped compounds. Though small, these changes illustrate that replacement of iron cations in octahedral coordination for gallium may result in a progressive decrease of the migration channel size. This consideration is supported by the increase in the activation energy in the low-temperature range where the ordered phases are formed (Table 4).

On the other hand, the variation in the activation energy values of single-phase $La_{0.3}Sr_{0.7}Fe_{1-x}Ga_xO_{3-\delta}$ ($x=0$–0.2) at temperatures above 850 °C is relatively small (Table 4). The large difference in the ionic conductivity of undoped and Ga-doped materials may thus suggest a considerable decrease in the ionic charge carrier concentration when gallium is incorporated into the iron sublattice. Exact reasons for such behaviour are still unclear. However, a similar phenomenon was found earlier for $La(Co,Ga)O_{3-\delta}$ solid solution, where ionic transport in the intermediate compositions was considerably lower than in both parent compounds, $LaCoO_{3-\delta}$ and $LaGaO_{3-\delta}$.[40] One possible explanation for this behaviour may be related to local distortions of the lattice near the guest gallium cations, resulting from the significant difference in covalence of Ga–O and Fe–O bonds. Such distortions may lead to blocking of oxygen anions neighbouring gallium cations, decreasing thus the mobile ion concentration.

The oxygen ion transference numbers (t_i) of the title materials, calculated from the data on partial conductivities (Table 2), are shown in Fig. 7 as functions of temperature, oxygen partial pressure and cation composition. Note that, strictly speaking, the data on ionic conductivity in Table 2 refer to the oxygen pressure range below 10^{-5} atm. For evaluation purposes they were extrapolated to the range of higher oxygen pressure and are therefore less reliable. The ion transference numbers vary from 1×10^{-3} to approximately 0.9, increasing with gallium concentration due to suppressed mobility of the electronic charge carriers when iron cations are substituted by gallium. At oxygen pressures higher than 10^{-12}–10^{-10} atm, the transference numbers increase with temperature, while at $pO_2<10^{-12}$ atm the behaviour is opposite. The latter trends are caused by the differences in the activation energies for partial ionic, p- and n-type electronic conductivities, as discussed above.

Table 4 Activation energy for oxygen ionic conduction in $La_{0.3}Sr_{0.7}Fe_{1-x}Ga_xO_{3-\delta}$ calculated in different temperature ranges

	E_i		
x	750–950 °C	750–850 °C	850–950 °C
0	0.82±0.03	0.88±0.03	0.76±0.06
0.1	1.04±0.07	1.24±0.02	0.78±0.02
0.2	1.3±0.1	1.56±0.04	0.91±0.06
0.4	1.25±0.04	1.37±0.04	1.09±0.04

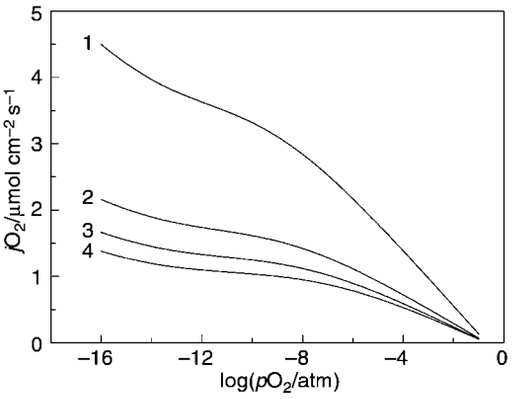

Fig. 8 Estimated oxygen permeation flux through $La_{0.3}Sr_{0.7}Fe_{1-x}Ga_xO_{3-\delta}$ membranes as a function of the permeate-side oxygen partial pressure at 900 °C. Membrane thickness is 1.0 mm. The feed-side oxygen partial pressure corresponds to atmospheric pressure. Numbers 1, 2, 3 and 4 correspond to the x values equal to 0, 0.1, 0.2 and 0.4, respectively.

Fig. 8 presents the estimations of oxygen permeation fluxes through $La_{0.3}Sr_{0.7}Fe_{1-x}Ga_xO_{3-\delta}$ membranes, calculated under assumption of a negligible effect of the oxygen surface exchange at oxide/gas boundaries on oxygen permeability. In these conditions, the oxygen flux density, jO_2, is determined by the well-known relationship[1,44]

$$jO_2=\frac{RT}{16F^2L}\int_{p''}^{p'}\sigma_{amb}\mathrm{d}\ \ln\ pO_2 \qquad (7)$$

where L is the membrane thickness, p' and p'' are the oxygen partial pressures at the membrane feed and permeate sides, respectively. The ambipolar conductivity, σ_{amb}, is defined as

$$\sigma_{amb}=\frac{\sigma_i(\sigma_n+\sigma_p)}{\sigma_i+\sigma_n+\sigma_p}\equiv\sigma(t_i-t_i^2) \qquad (8)$$

These estimations may give only an upper limit of oxygen permeation rate, since the presence of surface exchange limitations, typical for many $SrFeO_{3-\delta}$-based phases,[17] results in the suppression of oxygen transport. For the conditions typical for syngas generation (oxygen pressure gradient of 0.21×10^{-16} atm, 900 °C), the oxygen amount separated using a $La_{0.3}Sr_{0.7}FeO_{3-\delta}$ membrane with a thickness of 1.0 mm was estimated to achieve about 6 ml cm^{-2} min^{-1}. The decrease in both oxygen-ion and electron conductivities with increasing gallium content results in a lower permeation (Fig. 8); in the same conditions, oxygen fluxes through $La_{0.3}Sr_{0.7}Fe_{1-x}Ga_xO_{3-\delta}$ ($x=0.1$–0.4) membranes vary from 1.9 to approximately 3 ml cm^{-2} min^{-1}. Note that the permeation flux values between 2 and 3 ml cm^{-2} min^{-1} correspond to the maximum syngas production rate of 12–18 ml cm^{-2} min^{-1} in the methane partial oxidation process. For comparison, the rate of syngas production in a reactor with a tubular $La_{0.15}Sr_{0.85}Fe_{0.7}Ga_{0.3}O_{3-\delta}$ membrane at 900 °C was reported to vary in the range 13–15 ml cm^{-2} min^{-1}.[12] Thus, the obtained results on the conductivity of ferrites–gallates make possible a realistic estimation of the oxygen transport in membrane operation conditions.

Conclusions

Ceramic samples of Ga-doped lanthanum–strontium ferrite, $La_{0.3}Sr_{0.7}Fe_{1-x}Ga_xO_{3-\delta}$ ($x=0$–0.5), were synthesized and studied using X-ray diffraction, coulometric titration and total electrical conductivity measurements in the temperature

range 750–950 °C at oxygen partial pressures varying between 10^{-19} and 0.5 atm. The solid solubility limit of gallium in the $La_{0.3}Sr_{0.7}FeO_{3-\delta}$ lattice was found to be close to $x=0.3$; further increase in the gallium content results in segregation of the $SrLaGa_3O_7$ phase. The perovskite-type lattice of $La_{0.3}Sr_{0.7}(Fe,Ga)O_{3-\delta}$, stable in oxidizing conditions, transforms to oxygen-vacancy ordered structures at oxygen pressures about 10^{-4} atm. Doping with gallium leads to a transition from the brownmillerite-like structure (S.G. *Pmma*), characteristic of the reduced form of $La_{0.3}Sr_{0.7}FeO_{3-\delta}$, to an orthorhombic lattice (S.G. *Pmmm*) observed in reducing conditions for $La_{0.3}Sr_{0.7}Fe_{1-x}Ga_xO_{3-\delta}$ with $x>0$. Both p- and n-type electronic conductivities decrease when insulating gallium cations are incorporated into the iron sublattice of the ferrite. When oxygen partial pressure increases, the p-type conductivity of the vacancy-ordered phases changes from the intrinsic regime, when the electron–hole conduction is governed by the band gap, to the extrinsic regime, controlled by the amount of excess oxygen in the vacancy ordered structure. Oxygen ionic conductivity in the ordered phases decreases with increasing gallium concentration.

Acknowledgements

This work was partially supported by the Russian Foundation for Basic Research (grant no 98-03-3251a), by the FCT (Praxis, Portugal), and by the University of Aveiro.

References

1 H. J. M. Bouwmeester and A. J. Burgraaf, in *Fundamentals of Inorganic Membrane Science and Technology*, ed. A. J. Burgraaf and L. Cot, Elsevier, Amsterdam, 1996, p. 435.
2 W. Wang and Y. S. Lin, *J. Membr. Sci.*, 1995, **103**, 219.
3 J. Kilner, S. Benson, J. Lane and D. Waller, *Chem. Ind.*, 1997, **17**, 907.
4 T. J. Mazanec, *Solid State Ionics*, 1994, **70/71**, 11.
5 Y. Teraoka, H. M. Zhang, K. Okamoto and N. Yamazoe, *Mater. Res. Bull.*, 1988, **23**, 51.
6 R. M. Thorogood, R. Srinivasan, T. F. Yu and M. P. Drake, *US Patent* 5,240,480, 1993.
7 S. Carter, A. Selcuk, R. J. Chater, J. Kajda, J. A. Kilner and B. C. H. Steele, *Solid State Ionics*, 1992, **53–56**, 597.
8 W. J. Weber, J. W. Stevenson, T. R. Armstrong and L. R. Pederson, *Mater. Res. Soc. Symp. Proc.*, 1995, **369**, 395.
9 M. V. Patrakeev, I. A. Leonidov, E. B. Mitberg, A. A. Lakhtin, V. G. Vasiliev, V. L. Kozhevnikov and K. R. Poeppelmeier, *Ionics*, 1999, **5**, 444.
10 A. N. Petrov, V. A. Cherepanov, O. F. Kononchuk and L. Y. Gavrilova, *J. Solid State Chem.*, 1990, **87**, 69.
11 T. J. Mazanec, in *Ceramic Membranes I*, ed. H. U. Anderson, A. C. Krandhar and M. Liu, The Electrochemical Society, Pennington, NJ, PV95-24, 1997, p. 16.
12 M. Schwartz, J. White and A. Sammels, *Int. Patent Application* PCT WO 97/41060 1997.
13 S. Pei, M. S. Kleefisch, T. P. Kobylinsky, J. Faber, C. A. Udovich, V. Zhang-McCoy, B. D. Dabrowski, U. Balachandran, R. L. Mieville and R. B. Poeppel, *Catal. Lett.*, 1995, **30**, 201.
14 Q. Ming, M. D. Nersesyan, A. Wagner, J. Ritchie, J. T. Richardson, D. Luss, A. J. Jacobson and Y. L. Yang, *Solid State Ionics*, 1999, **122**, 113.
15 T. J. Mazanec, T. L. Cable, J. G. Frye and W. R. Kliewer, *US Patent* 5,591,315, 1997.
16 Q. Ming, J. Hung, Y. L. Yang, M. D. Nersesyan, A. J. Jacobson, J. T. Richardson and D. Luss, *Combust. Sci. Technol.*, 1998, **138**, 279.
17 V. V. Kharton, A. P. Viskup, A. V. Kovalevsky, J. R. Jurado, E. N. Naumovich, A. A. Vecher and J. R. Frade, *Solid State Ionics*, 2000, **133**, 57.
18 T. R. Armstrong, J. W. Stevenson, K. Hasinska and D. E. McReady, *J. Electrochem. Soc.*, 1998, **145**, 4282.
19 P. Karen and T. Norby, *J. Electrochem. Soc.*, 1998, **145**, 264.
20 V. V. Kharton, V. V. Astashko, P. P. Zhuk, A. K. Demin, A. A. Tonoyan, M. P. Gilevich and A. A. Vecher, *Vestsi AN Belarusi, Ser. Khim.*, 1992, **3/4**, 70 [in Russian].
21 V. V. Kharton, A. A. Yaremchenko, A. V. Kovalevsky, A. P. Viskup, E. N. Naumovich and P. F. Kerko, *J. Membr. Sci.*, 1999, **163**, 307.
22 M. V. Patrakeev, I. A. Leonidov, A. A. Lakhtin, E. B. Mitberg and V. L. Kozhevnikov, *Zh. Fiz. Khim.*, 1996, **70**, 611 [in Russian].
23 V. L. Kozhevnikov, I. A. Leonidov, M. V. Patrakeev, E. B. Mitberg and K. R. Poeppelmeier, *J. Solid State Chem.*, 2000, submitted.
24 J. Rodriguez-Carvajal, in *Satellite Meeting on Powder Diffraction*, Abstr. XVth Conf. of the Int. Union of Crystallography, Toulouse, 1990, p. 127.
25 M. V. Patrakeev, E. B. Mitberg, A. A. Lakhtin, I. A. Leonidov, V. L. Kozhevnikov and K. R. Poeppelmeier, *Ionics*, 1998, **4**, 191.
26 E. B. Mitberg, M. V. Patrakeev, A. A. Lakhtin, I. A. Leonidov, V. L. Kozhevnikov and K. R. Poeppelmeier, *J. Alloys Compd.*, 1998, **274**, 103.
27 F. M. B. Marques and G. P. Wirtz, *J. Am. Ceram. Soc.*, 1992, **75**, 369.
28 Powder Diffraction File, Card 45-0637, JCPDS International Center Diffraction Data, 12 Campus Boulevard, Newtown Square, PA 19073-3273, USA.
29 N. Trofimenko and H. Ullmann, *Solid State Ionics*, 1999, **118**, 215.
30 M. Abbate, F. M. F. de Groot, J. C. Fuggle, A. Furimoto, O. Strebel, F. Lopez, M. Domke, G. Kaindl, G. A. Sawadsky, M. Takano, Y. Takeda, H. Eisaki and S. Uchida, *Phys. Rev. B*, 1992, **46**, 4511.
31 G. R. Hearne, M. P. Pasternak, R. D. Taylor and P. Lacorre, *Phys. Rev. B*, 1995, **51**, 11495.
32 R. D. Shannon, *Acta Crystallogr., Sect. A*, 1976, **32**, 751.
33 J.-C. Grenier, N. Ea, M. Pouchard and P. Hagenmuller, *J. Solid State Chem.*, 1985, **58**, 243.
34 A. R. West, *Solid State Chemistry and Its Applications*, Wiley, Chichester, 1984.
35 P. D. Battle, T. C. Gibb and P. Lightfoot, *J. Solid State Chem.*, 1990, **84**, 271.
36 P. D. Battle, T. C. Gibb and P. Lightfoot, *J. Solid State Chem.*, 1990, **84**, 237.
37 J. P. Hodges, S. Short, J. D. Jorgensen, X. Xiong, B. Dabrovski, S. M. Mini and C. W. Kimball, *J. Solid State Chem.*, 2000, **151**, 190.
38 Y. Takeda, K. Kanno, T. Takada, O. Yamamoto, M. Takano, N. Nakayama and Y. Bando, *J. Solid State Chem.*, 1986, **63**, 237.
39 S. Wissmann and K. D. Becker, *Solid State Ionics*, 1996, **85**, 279.
40 V. V. Kharton, A. P. Viskup, E. N. Naumovich and N. M. Lapchuk, *Solid State Ionics*, 1997, **104**, 67.
41 J. Mizusaki, T. Sasamoto, W. R. Cannon and H. K. Bowen, *J. Am. Ceram. Soc.*, 1982, **65**, 363.
42 J. Mizusaki, T. Sasamoto, W. R. Cannon and H. K. Bowen, *J. Am. Ceram. Soc.*, 1983, **66**, 247.
43 S. Steinsvik, R. Bugge, J. Gjønnes, J. Taftø and T. Norby, *J. Phys. Chem. Solids*, 1997, **58**, 969.
44 H. Schmalzried, *Solid State Reactions*, 2nd edn., Verlag Chemie, Weinheim, 1981.